Digit. Signal Process. 156 (2025) 104799

Contents lists available at ScienceDirect

Digital Signal Processing

journal homepage: www.elsevier.com/locate/dsp

IRS aided visible light positioning with a single LED transmitter

Efe Tarhan [a], Furkan Kokdogan [b], Sinan Gezici [a,*]

[a] Department of Electrical and Electronics Engineering, Bilkent University, Ankara 06800, Turkey
[b] ASML, Eindhoven, Netherlands

ARTICLE INFO

Keywords:
Intelligent reflecting surface
Visible light positioning
Estimation
Cramér-Rao lower bound

ABSTRACT

We propose a visible light positioning (VLP) system with a single light emitting diode (LED) transmitter and an intelligent reflecting surface (IRS) for estimating the position of a receiver equipped with a single photodetector. By performing a number of transmissions from the LED transmitter and optimizing the orientation vectors of the IRS elements for each transmission, position information is extracted by the receiver based on power measurements of the signals reflecting from the IRS. The theoretical limit and the maximum likelihood (ML) estimator are presented for the proposed setting. In addition, an algorithm, named IRS focusing, is proposed for determining the orientations of the IRS elements during the localization process. The effectiveness of the proposed localization approach is demonstrated through simulations. Furthermore, extensions are provided to apply the proposed approach in the presence of partial prior information about the receiver position and when the IRS is located at the LED transmitter.

1. Introduction

With origins in semiconductor research, the advancement of light emitting diodes (LEDs) has made a notable contribution to optical communication and lighting technology. These devices have transitioned from simple signal indicators to sophisticated means for transmitting information efficiently across distances, accompanied by reduced energy consumption. In the context of visible light communication (VLC) systems, LEDs serve to modulate light for data transmission at rates not perceivable to the human eye, offering a viable alternative in environments where traditional radio frequency (RF) communication is impeded by interference or regulatory limitations. The attributes of LEDs, namely, energy efficiency, durability, and cost-effectiveness, have broadened their applications from basic lighting to high-speed internet access through Li-Fi and intricate signaling systems [1–5]. Furthermore, LED transmitters are instrumental in visible light positioning (VLP) systems [6–9]. These systems leverage the intensity or delay of light from LEDs to determine precise indoor locations, providing a robust solution for navigation and location-based services where GPS is ineffective. The adoption of the LED technology in VLP systems underscores its potential for innovation in sectors such as retail, healthcare and smart building management, highlighting the extensive impact of LED technology across various domains. This has led to innovative uses of LEDs in indoor VLP systems, and numerous studies have proposed position estimation algorithms and explored theoretical limits for localization accuracy [6,10–13].

In the domain of VLP systems, received signal strength (RSS) has emerged as a fundamental metric, facilitating cost-effective and accurate localization methods [12]. Leveraging the intensity modulation of light emitted by LED transmitters, RSS-based techniques estimate the position of a VLC receiver, offering simplicity and minimal computational cost. This approach is especially valuable for applications such as indoor navigation and asset tracking in GPS-inadequate environments [14]. A key factor in specifying the accuracy of RSS-based positioning is the application of the Cramér-Rao lower bound (CRLB), which provides a theoretical benchmark for the minimum variance that can be achieved by unbiased estimators. In VLP systems, CRLB calculations allow for the quantification of the utmost accuracy limits for position estimations derived from RSS measurements. A notable contribution in this field is the development of a generic closed-form expression for the CRLB, which quantifies the accuracy of localization algorithms based on RSS measurements [15]. In [9], the effects of luminous flux degradation of LEDs on localization accuracy are investigated by deriving the misspecified Cramér-Rao bound (MCRB) and the mismatched maximum likelihood (MML) estimator.

Intelligent reflecting surfaces (IRSs), also called reconfigurable intelligent surfaces (RISs), have emerged as a transformative technology for RF communications and localization systems. An IRS is composed

* Corresponding author.
E-mail addresses: efe.tarhan@ug.bilkent.edu.tr (E. Tarhan), kokdoganfurkan@gmail.com (F. Kokdogan), gezici@ee.bilkent.edu.tr (S. Gezici).

https://doi.org/10.1016/j.dsp.2024.104799

Available online 10 October 2024
1051-2004/

of small, low-cost passive elements that are capable of altering the phase, direction, amplitude, and/or frequency of RF signals. The development and capabilities of IRSs are thoroughly reviewed in the literature [16]. One notable application of IRS is beamforming, which allows for the redirection of electromagnetic waves in specific directions. The enhancement of wireless communications through the use of IRSs, including proposed algorithms for joint active and passive beamforming to optimize signal power at the user, is discussed in [17]. These algorithms have shown significant performance gains in simulated scenarios. In addition, [18] introduces two iterative algorithms aimed at improving energy efficiency in single-user and multi-user scenarios, presenting notable advancements over traditional IRS approaches.

Research on IRS-based VLC systems has also been prolific [19–22]. Abdelhady et al. discuss the light reflection models from IRS elements in metasurface and mirror array-based structures, establishing a baseline for further investigation, particularly in point source cases as outlined in [19]. Furthermore, Hanaa Abumarshood et al. have developed a joint optimization scheme for non-orthogonal multiple access (NOMA) decoding order, power allocation, and IRS reflection coefficients to enhance the bit error rate (BER) performance in VLC systems [20]. This scheme is particularly effective in scenarios involving blockages and random device orientations, as explored in [20]. The application of IRSs in wireless positioning systems has also been a focal point of recent studies, with research addressing the use of multiple IRSs in scenarios lacking sufficient transmitters, as well as several proposed device-to-device localization schemes for RF communication using IRSs, which are discussed in [23–27].

Optimization techniques are crucial for improving the performance and accuracy of VLP and VLC systems, particularly with the advent of IRS. Chen et al. provide a thorough analysis of various optimization models for three-dimensional VLP systems, focusing on critical parameters that influence accuracy and efficiency, serving as a benchmark for understanding and improving VLP system performance [28]. Also, Meng et al. extend these principles by implementing an improved whale optimization algorithm specifically tailored for indoor high-precision 3D positioning systems utilizing visible light, demonstrating notable advancements in positioning accuracy and system robustness [29]. The role of IRS in enhancing VLP and VLC systems is comprehensively surveyed in [30] by exploring a variety of optimization techniques that harness the potential of IRS to enhance the performance and efficiency of 6G wireless networks. Wu et al. further investigate the capacity maximization in IRS-aided multiple-input single-output (MISO) VLC systems, employing advanced optimization strategies that significantly improve data throughput, thereby demonstrating the substantial impact of IRS on communication capabilities within VLC systems [31]. Additionally, Yang et al. focus on maximizing the average signal-to-noise ratio (SNR) in IRS-aided indoor VLC systems using genetic algorithms and neural networks, highlighting the effectiveness of sophisticated computational techniques in optimizing communication system performance [32].

Although IRSs have been considered for VLC systems in various studies such as [19–22], IRS aided VLP systems have not been investigated thoroughly in the literature. In [33], multiple LED transmitters and IRSs are utilized to perform position estimation based on RSS measurements for determining the position of a VLC receiver in the absence of line-of-sight (LOS) signals, and orientations of IRS elements are adjusted towards the VLC receiver for improving localization accuracy. In addition, [34] extends the scenario in [33] by taking into account possible mismatches between the assumed and true orientations of the IRS elements (mirrors), and investigates the degradation of localization accuracy due to orientation mismatches based on an MCRB analysis. In this manuscript, we employ a novel approach for estimating the position of a fixed VLC receiver with a single photo-detector by utilizing a single LED transmitter and a mirror-array based IRS. In particular, we optimize the orientations of the IRS elements (mirrors) over a number of time intervals so that position related information can be extracted from received power measurements at the VLC receiver based on signals sent from the LED and coming from the IRS. We also present the CRLB and the maximum likelihood (ML) estimator for the proposed setting. We show that by designing IRS orientations (called IRS profiles) in an efficient manner, accurate position estimation can be performed with a single LED transmitter and an IRS. We also extend the results to practical scenarios with partial prior information about the position of the VLC receiver, and propose a position estimation approach for VLP systems with a single LED transmitter which is equipped with an IRS (i.e., when the IRS is at the transmitter). It is important to emphasize that the approach in [33] (or, [34]), which proposes to focus IRSs towards the VLC receiver, cannot be employed for the single LED transmitter and the single IRS scenario considered in this manuscript. Also, the idea of VLP with a single LED transmitter equipped with an IRS has not been available in the literature. The main technical contributions and novelty of this manuscript can be stated as follows:

- We propose an approach for estimating the position of a fixed VLC receiver with a single photo-detector in the presence of a single LED transmitter and an IRS for the first time in the literature.
- We present the CRLB and the ML estimator for the proposed setting.
- We propose an "IRS focusing" algorithm for determining the orientation vectors of the IRS elements in order to reduce the CRLB for position estimation.
- We also propose a localization approach in the presence of a single LED transmitter when the IRS is at the transmitter by optimizing the orientation vector of the LED transmitter in a number of time intervals.

We also compare the localization performance of the proposed IRS focusing approach with random and aligned IRS profiles via simulations.

The structure of this paper is as follows: Section 2 details the channel model for the VLP system in an indoor environment with a single LED transmitter and an IRS, including essential formulas that describe the relationship between transmitted and received powers. In addition, the CRLB and the ML estimator are derived. In Section 3, we present the proposed approach for determining the orientation vectors of the IRS elements, as well as two benchmark techniques for comparison purposes. Alternative problems that can be investigated are placed in Section 4, including possible extensions to the proposed approaches. Section 5 describes the simulation setup and results, illustrating the effectiveness of the proposed localization approach. Final remarks and conclusions are made in Section 6.

2. IRS aided VLP with single LED

We investigate a VLP system with a single LED transmitter at a known location denoted by $\boldsymbol{l}$ and a VLC receiver with a single photo-detector at an unknown location represented by $\boldsymbol{x}$, where $\boldsymbol{l} \in \mathbb{R}^3$ and $\boldsymbol{x} \in \mathbb{R}^3$. As in [33] and [35], we assume that the orientation vectors of the LED transmitter and the VLC receiver are known, and we denote them by $\boldsymbol{n} \in \mathbb{R}^3$ and $\bar{\boldsymbol{n}} \in \mathbb{R}^3$, respectively. In addition to the VLC receiver and the LED transmitter, there exists an IRS in the environment, which consists of N_{R} flat surface elements (mirrors) represented by $S_1, \ldots, S_{N_{\mathrm{R}}}$ at known locations $\tilde{\boldsymbol{l}}_1, \ldots, \tilde{\boldsymbol{l}}_{N_{\mathrm{R}}}$. The orientation vectors of the IRS elements can be adjusted for localization purposes and each given a set of orientation vectors is called an *IRS profile*. We assume that there exist N_{P} IRS profiles and the orientation vectors of the IRS elements are denoted by $\tilde{\boldsymbol{n}}_1^{(i)}, \ldots, \tilde{\boldsymbol{n}}_{N_{\mathrm{R}}}^{(i)}$ for the ith IRS profile, where $i \in \{1, \ldots, N_{\mathrm{P}}\}$. Each IRS element is modeled to cause glossy reflections (i.e., Phong's model) [19,36] and the reflectance coefficient is assumed to remain constant over each given surface; that is, ρ_k is used to represent the reflectance coefficient for the kth IRS element with $k \in \{1, \ldots, N_{\mathrm{R}}\}$. As the IRS is considered as a part of the system design, $\tilde{\boldsymbol{n}}_k^{(i)}$, ρ_k, and S_k (i.e., the surface equation) are assumed to be known by the VLC receiver for all $k \in \{1, \ldots, N_{\mathrm{R}}\}$ and $i \in \{1, \ldots, N_{\mathrm{P}}\}$ [33]. The considered system model is shown in Fig. 1.

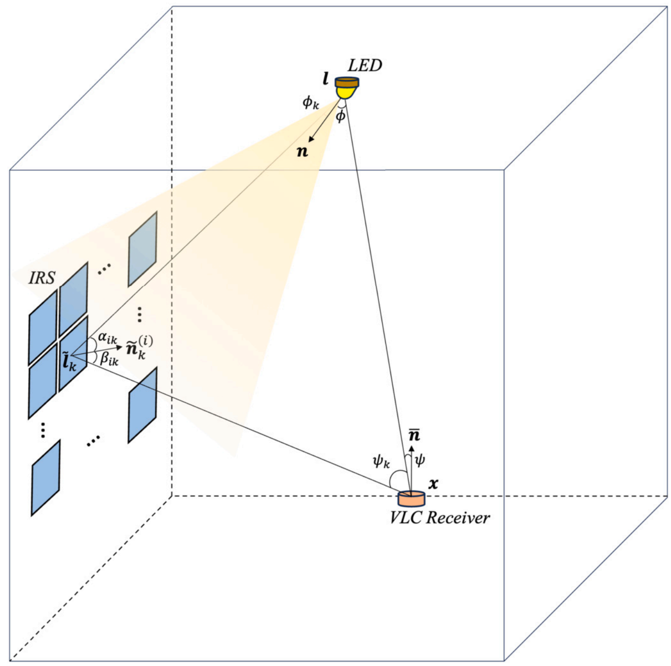

Fig. 1. A visible light system with a single LED transmitter, an IRS with N_R elements, and a VLC receiver with a single photo-detector.

The aim is to estimate the unknown location $\boldsymbol{x}$ of the VLC receiver based on power measurements at the VLC receiver due to the signals emitted by the LED transmitter by using N_P different IRS profiles. Namely, N_P power measurements are taken by the VLC receiver in N_P consecutive time slots, where a distinct and known IRS profile is used in each slot.[1] In this scenario, the received power measurement at the VLC receiver corresponding to the ith IRS profile can be modeled as follows [33]:

$$P_{\mathrm{RX},i} = P_\mathrm{TX} H^\mathrm{LOS}(\boldsymbol{x}) + P_\mathrm{TX} \sum_{k=1}^{N_\mathrm{R}} \int_{S_k} d H^\mathrm{ref}_{i,k}\left(\boldsymbol{x}, \tilde{\boldsymbol{n}}_k^{(i)}\right) + \eta_i \tag{1}$$

for $i = 1, \ldots, N_\mathrm{P}$, where P_TX is the transmit power of the LED transmitter, $H^\mathrm{LOS}(\boldsymbol{x})$ is the channel gain of the LOS path between the LED transmitter and the VLC receiver, $dH^\mathrm{ref}_{i,k}\left(\boldsymbol{x}, \tilde{\boldsymbol{n}}_k^{(i)}\right)$ is the channel gain of the path between the LED transmitter and the VLC receiver which makes a single reflection from an infinitesimal area around $\tilde{\boldsymbol{l}}_k$ at the kth IRS element (please see Fig. 1), and η_i is a zero-mean Gaussian noise component with a variance of σ_i^2, which is independent of η_j for all $j \neq i$ [37].

We adopt the same room setup as in [33]; namely, we assume that the field-of-view (FOV) of the photo-detector at the VLC receiver is 90^o [19] (i.e., a hemispherical lens is used at the VLC receiver [38]) and that the VLC receiver is at a lower height than the IRS and the LED. Then, by following similar steps to those in [33, Sec. II], the channel gains in (1) can be expressed as

$$H^\mathrm{LOS}(\boldsymbol{x}) = \frac{(m+1)A\left((\boldsymbol{x}-\boldsymbol{l})^T \boldsymbol{n}\right)^m (\boldsymbol{l}-\boldsymbol{x})^T \bar{\boldsymbol{n}}}{2\pi \|\boldsymbol{x}-\boldsymbol{l}\|^{m+3}} \tag{2}$$

$$dH^\mathrm{ref}_{i,k}\left(\boldsymbol{x}, \tilde{\boldsymbol{n}}_k^{(i)}\right) = \frac{(m+1)\left((\tilde{\boldsymbol{l}}_k-\boldsymbol{l})^T \boldsymbol{n}\right)^m \left((\boldsymbol{l}-\tilde{\boldsymbol{l}}_k)^T \tilde{\boldsymbol{n}}_k^{(i)}\right)}{4\pi^2 \|\boldsymbol{l}-\tilde{\boldsymbol{l}}_k\|^{m+3} \|\boldsymbol{x}-\tilde{\boldsymbol{l}}_k\|^3}$$

$$A\rho_k\left((\tilde{\boldsymbol{l}}_k - \boldsymbol{x})^T \bar{\boldsymbol{n}}\right) dS_k \Bigg(2r_k \frac{(\boldsymbol{x}-\tilde{\boldsymbol{l}}_k)^T \tilde{\boldsymbol{n}}_k^{(i)}}{\|\boldsymbol{x}-\tilde{\boldsymbol{l}}_k\|} + (1-r_k)(\mu_k+1)(\cos(\beta_{ik}-\alpha_{ik}))^{\mu_k}\Bigg) \tag{3}$$

with

$$\cos(\beta_{ik}-\alpha_{ik}) = \frac{\left((\boldsymbol{x}-\tilde{\boldsymbol{l}}_k)^T \tilde{\boldsymbol{n}}_k^{(i)}\right)\left((\boldsymbol{l}-\tilde{\boldsymbol{l}}_k)^T \tilde{\boldsymbol{n}}_k^{(i)}\right)}{\|\boldsymbol{x}-\tilde{\boldsymbol{l}}_k\| \|\boldsymbol{l}-\tilde{\boldsymbol{l}}_k\|} + \frac{\left\|(\boldsymbol{x}-\tilde{\boldsymbol{l}}_k)\times \tilde{\boldsymbol{n}}_k^{(i)}\right\| \left\|(\boldsymbol{l}-\tilde{\boldsymbol{l}}_k)\times \tilde{\boldsymbol{n}}_k^{(i)}\right\|}{\|\boldsymbol{x}-\tilde{\boldsymbol{l}}_k\| \|\boldsymbol{l}-\tilde{\boldsymbol{l}}_k\|} \tag{4}$$

where $\times$ represents the cross product. In (2) and (3), A denotes the surface area of the photo detector at the VLC receiver, m is the Lambertian order of the LED transmitter (determines the spatial concentration of the emitted light), ρ_k stands for the reflectivity constant of the mirror elements at the IRS (the fraction of the transmitted light power in the comparison to the incoming power), the parameter $r_k \in [0,1]$ denotes the fraction of the diffuse component of the light reflected from the mirrors, and μ_k determines the directivity of the specular component of the reflected light, which corresponds to the $(1-r_k)$ portion of the total reflected light in (3) [36].

Let $\boldsymbol{P}_\mathrm{RX}$ denote the set of received powers in (1), that is, $\boldsymbol{P}_\mathrm{RX} = [P_{\mathrm{RX},1} \cdots P_{\mathrm{RX},N_\mathrm{P}}]$. Based on $\boldsymbol{P}_\mathrm{RX}$, the log-likelihood function for the unknown location $\boldsymbol{x}$ of the VLC receiver can be expressed as

$$\log p(\boldsymbol{P}_\mathrm{RX} \,|\, \boldsymbol{x}) = \tilde{k} - \sum_{i=1}^{N_\mathrm{P}} \frac{1}{2\sigma_i^2}\Bigg(P_{\mathrm{RX},i} - P_\mathrm{TX} H^\mathrm{LOS}(\boldsymbol{x}) - P_\mathrm{TX} \sum_{k=1}^{N_\mathrm{R}} \int_{S_k} dH^\mathrm{ref}_{i,k}\left(\boldsymbol{x}, \tilde{\boldsymbol{n}}_k^{(i)}\right)\Bigg)^2 \tag{5}$$

where $\tilde{k}$ is a constant independent of $\boldsymbol{x}$. Then, the ML estimator for the location of the VLC receiver can be expressed as follows:

$$\hat{\boldsymbol{x}}_\mathrm{ML} = \arg\min_{\boldsymbol{x}} \sum_{i=1}^{N_\mathrm{P}} \frac{1}{\sigma_i^2}\Bigg(P_{\mathrm{RX},i} - P_\mathrm{TX} H^\mathrm{LOS}(\boldsymbol{x}) - P_\mathrm{TX} \sum_{k=1}^{N_\mathrm{R}} \int_{S_k} dH^\mathrm{ref}_{i,k}\left(\boldsymbol{x}, \tilde{\boldsymbol{n}}_k^{(i)}\right)\Bigg)^2 \tag{6}$$

where H^LOS and $dH^\mathrm{ref}_{i,k}$ are evaluated based on (2)–(4).

The CRLB derivations in [33] can also be modified to obtain the CRLB for the considered VLP problem with a single LED transmitter. Namely, the elements of the Fisher information matrix (FIM) [39], denoted by $\mathbf{I}(\boldsymbol{x})$, can be calculated from (5), as follows:

$$[\mathbf{I}(\boldsymbol{x})]_{\ell_1,\ell_2} = (P_\mathrm{TX})^2 \sum_{i=1}^{N_\mathrm{P}} \frac{1}{\sigma_i^2} \frac{\partial h_i(\boldsymbol{x})}{\partial x_{\ell_1}} \frac{\partial h_i(\boldsymbol{x})}{\partial x_{\ell_2}} \tag{7}$$

for $\ell_1, \ell_2 \in \{1,2,3\}$, where

$$h_i(\boldsymbol{x}) \triangleq H^\mathrm{LOS}(\boldsymbol{x}) + \sum_{k=1}^{N_\mathrm{R}} \int_{S_k} dH^\mathrm{ref}_{i,k}\left(\boldsymbol{x}, \tilde{\boldsymbol{n}}_k^{(i)}\right). \tag{8}$$

Then, the partial derivatives of $h_i(\boldsymbol{x})$ in (8) can be expressed as

$$\frac{\partial h_i(\boldsymbol{x})}{\partial x_\ell} = \frac{\partial H^\mathrm{LOS}(\boldsymbol{x})}{\partial x_\ell} + \sum_{k=1}^{N_\mathrm{R}} \int_{S_k} \frac{\partial\, dH^\mathrm{ref}_{i,k}\left(\boldsymbol{x}, \tilde{\boldsymbol{n}}_k^{(i)}\right)}{\partial x_\ell} \tag{9}$$

for $i \in \{1, \ldots, N_\mathrm{P}\}$ and $\ell \in \{1,2,3\}$.

Remark 1. In the absence of the IRS (i.e., in the absence of the second term in (9)), the FIM specified by (7) becomes a rank-one matrix, leading to an infinite CRLB. Hence, accurate position estimation is not possible

[1] It is assumed that the mobility of the VLC receiver is negligible during these time slots, which is a reasonable assumption for indoor localization scenarios. Since speed of movement is limited for indoor environments, channel coherence time is longer and there exists a longer time to perform position estimation in indoor systems compared to that in outdoor systems such as vehicular networks.

in that case. This is intuitive since only distance related information can be obtained from LOS power measurements between a single LED transmitter and a fixed VLC receiver with a single photo-detector. □

Remark 2. As the positioning accuracy depends on the sensitivity of the power measurements from the IRS to the unknown position parameter $\boldsymbol{x}$, it is reasonable to direct the LED transmitter towards the IRS so that the IRS elements get and reflect more powerful signals, as shown in Fig. 1. It should be emphasized that although the LOS component is degraded when the LED points towards the IRS, we still take into account the signals due to the LOS path.[2] □

From the expressions in (2)–(4), the partial derivatives in (9) can be evaluated as in [33] by considering the fact that there is a single LED transmitter but N_{P} orientation vectors for each IRS element:

$$\frac{\partial H^{\mathrm{LOS}}(\boldsymbol{x})}{\partial x_\ell} = \frac{-(m+1)A}{2\pi\|\boldsymbol{x}-\boldsymbol{l}\|^{m+3}}\Bigg[\bar{n}_\ell\left((\boldsymbol{x}-\boldsymbol{l})^T\boldsymbol{n}\right)^m - mn_\ell\left((\boldsymbol{x}-\boldsymbol{l})^T\boldsymbol{n}\right)^{m-1}(\boldsymbol{l}-\boldsymbol{x})^T\bar{\boldsymbol{n}} + \frac{(m+3)(x_\ell-l_\ell)\left((\boldsymbol{x}-\boldsymbol{l})^T\boldsymbol{n}\right)^m(\boldsymbol{l}-\boldsymbol{x})^T\bar{\boldsymbol{n}}}{\|\boldsymbol{x}-\boldsymbol{l}\|^2}\Bigg], \tag{10}$$

$$\frac{\partial dH^{\mathrm{ref}}_{i,k}\left(\boldsymbol{x},\tilde{\boldsymbol{n}}_k^{(i)}\right)}{\partial x_\ell} = \frac{(m+1)A\left((\tilde{\boldsymbol{l}}_k-\boldsymbol{l})^T\boldsymbol{n}\right)^m(\boldsymbol{l}-\tilde{\boldsymbol{l}}_k)^T\tilde{\boldsymbol{n}}_k^{(i)}}{4\pi^2\|\boldsymbol{l}-\tilde{\boldsymbol{l}}_k\|^{m+3}}$$
$$\rho_k dS_k\Bigg\{\Bigg[\left(\tilde{n}^{(i)}_{k,\ell}(\tilde{\boldsymbol{l}}_k-\boldsymbol{x})^T\bar{\boldsymbol{n}} - \bar{n}_\ell((\boldsymbol{x}-\tilde{\boldsymbol{l}}_k)^T\tilde{\boldsymbol{n}}_k^{(i)}\right)\|\boldsymbol{x}-\tilde{\boldsymbol{l}}_k\|^{-4} - 4\|\boldsymbol{x}-\tilde{\boldsymbol{l}}_k\|^{-6}(x_\ell-\tilde{l}_{k,\ell})(\boldsymbol{x}-\tilde{\boldsymbol{l}}_k)^T\tilde{\boldsymbol{n}}_k^{(i)}(\tilde{\boldsymbol{l}}_k-\boldsymbol{x})^T\bar{\boldsymbol{n}}\Bigg]2r_k$$
$$+(1-r_k)(\mu_k+1)\Bigg[(\cos(\beta_{ik}-\alpha_{ik}))^{\mu_k}\left(-\bar{n}_\ell\|\boldsymbol{x}-\tilde{\boldsymbol{l}}_k\|^{-3} - 3(\tilde{\boldsymbol{l}}_k-\boldsymbol{x})^T\bar{\boldsymbol{n}}\|\boldsymbol{x}-\tilde{\boldsymbol{l}}_k\|^{-5}(x_\ell-\tilde{l}_{k,\ell})\right) + \mu_k(\cos(\beta_{ik}-\alpha_{ik}))^{\mu_k-1}\frac{(\tilde{\boldsymbol{l}}_k-\boldsymbol{x})^T\bar{\boldsymbol{n}}}{\|\boldsymbol{x}-\tilde{\boldsymbol{l}}_k\|^3}\frac{\partial\cos(\beta_{ik}-\alpha_{ik})}{\partial x_\ell}\Bigg]\Bigg\} \tag{11}$$

with

$$\frac{\partial\cos(\beta_{ik}-\alpha_{ik})}{\partial x_\ell} = \cos\alpha_{ik}\left(\tilde{n}^{(i)}_{k,\ell}\|\boldsymbol{x}-\tilde{\boldsymbol{l}}_k\|^{-1} - (\boldsymbol{x}-\tilde{\boldsymbol{l}}_k)^T\tilde{\boldsymbol{n}}_k^{(i)}\|\boldsymbol{x}-\tilde{\boldsymbol{l}}_k\|^{-3}(x_\ell-\tilde{l}_{k,\ell})\right)+$$
$$\sin\alpha_{ik}\Big(\left\|(\boldsymbol{x}-\tilde{\boldsymbol{l}}_k)\times\tilde{\boldsymbol{n}}_k^{(i)}\right\|^{-1}\Big\{\tilde{n}^{(i)}_{k,f(\ell+1)}\left[(x_\ell-\tilde{l}_{k,\ell})\tilde{n}^{(i)}_{k,f(\ell+1)} - (x_{f(\ell+1)}-\tilde{l}_{k,f(\ell+1)})\tilde{n}^{(i)}_{k,\ell}\right] - \tilde{n}^{(i)}_{k,f(\ell+2)}\left[(x_{f(\ell+2)}-\tilde{l}_{k,f(\ell+2)})\tilde{n}^{(i)}_{k,\ell} - (x_\ell-\tilde{l}_{k,\ell})\tilde{n}^{(i)}_{k,f(\ell+2)}\right]\Big\}$$
$$\|\boldsymbol{x}-\tilde{\boldsymbol{l}}_k\|^{-1} - \|\boldsymbol{x}-\tilde{\boldsymbol{l}}_k\|^{-3}(x_\ell-\tilde{l}_{k,l})\left\|(\boldsymbol{x}-\tilde{\boldsymbol{l}}_k)\times\tilde{\boldsymbol{n}}_k^{(i)}\right\|\Big) \tag{12}$$

for $\ell\in\{1,2,3\}$, where $\bar{n}_\ell$, n_ℓ, x_ℓ, l_ℓ, $\tilde{n}^{(i)}_{k,\ell}$, and $\tilde{l}_{k,\ell}$ correspond to the ℓth components of vectors $\bar{\boldsymbol{n}}$, $\boldsymbol{n}$, $\boldsymbol{x}$, $\boldsymbol{l}$, $\tilde{\boldsymbol{n}}_k^{(i)}$, and $\tilde{\boldsymbol{l}}_k$, respectively, and $f(\ell)$ is given by $f(\ell)=\ell$ if $\ell\le 3$ and $f(\ell)=\ell-3$ otherwise. In addition, the $\cos\alpha_{ik}$ and $\sin\alpha_{ik}$ terms in (12) can be calculated from the relation $(\boldsymbol{l}-\tilde{\boldsymbol{l}}_k)^T\tilde{\boldsymbol{n}}_k^{(i)} = \|\boldsymbol{l}-\tilde{\boldsymbol{l}}_k\|\cos\alpha_{ik}$ [33].

Via the expressions in (4), (7), and (9)–(12), the CRLB, which is the trace of the inverse of the FIM can be obtained. The CRLB provides a limit on the mean-squared error (MSE) of any unbiased position estimator $\hat{\boldsymbol{x}}$ as $\mathrm{E}\{\|\hat{\boldsymbol{x}}-\boldsymbol{x}\|^2\}\ge\mathrm{trace}\{\mathbf{I}(\boldsymbol{x})^{-1}\}$. Therefore, the estimation accuracy limit can be specified without implementing a specific estimator, which is a useful tool while determining system parameters. Also, when the first term in (9) is set to zero, the CRLB in the absence of the LOS component can be obtained.

3. Selection of IRS profiles

In this section, we propose an IRS profile selection strategy for determining the N_{P} IRS profiles to be employed during localization in order to achieve accurate position estimation for the setup described in Section 2.

As the MSE of the ML estimator converges to the CRLB at high SNRs, one approach is to determine the N_{P} IRS profiles that minimize the CRLB for estimating the position $\boldsymbol{x}$ of the VLC receiver. In that case, the following optimization problem can be considered:

$$\underset{\left\{\tilde{\boldsymbol{n}}_k^{(i)}\right\}_{k=1,i=1}^{N_{\mathrm{R}},N_{\mathrm{P}}}}{\text{minimize}}\ \mathrm{trace}\{\mathbf{I}(\boldsymbol{x})^{-1}\} \tag{13}$$
$$\text{subject to}\ \left\|\tilde{\boldsymbol{n}}_k^{(i)}\right\|=1,\ k\in\{1,\dots,N_{\mathrm{R}}\},\ i\in\{1,\dots,N_{\mathrm{P}}\}$$

where the FIM, $\mathbf{I}(\boldsymbol{x})$, is calculated as defined in the previous section. The problem in (13) requires optimization over $2N_{\mathrm{R}}N_{\mathrm{P}}$ variables (after incorporating the constraints). As the number of elements in an IRS is usually very high, (13) has prohibitive complexity in general. Therefore, we propose an approach based on *IRS focusing*; namely, we aim to determine N_{P} locations in the positioning environment (in an optimal manner) and to focus the IRS elements towards those locations for different IRS profiles. The idea behind this approach is that by focusing the IRS to a set of suitably selected locations in an environment, accurate position information can be extracted from the power measurements corresponding to different IRS profiles (i.e., different focus locations).

To describe the proposed approach, let $\bar{\boldsymbol{l}}_i$ denote the focus location for the ith IRS profile, where $i\in\{1,\dots,N_{\mathrm{P}}\}$. In other words, the IRS elements focus their signals towards location $\bar{\boldsymbol{l}}_i$ for the ith IRS profile in the sense that the total received power is maximized at $\bar{\boldsymbol{l}}_i$ by adjusting the orientations of the IRS elements, which can be performed in a low complexity manner as described in [33, Sec. III]. Let those known mappings between the focus location $\bar{\boldsymbol{l}}_i$ and the orientation vectors of the IRS elements be denoted by functions $g_k(\cdot)$ such that $\tilde{\boldsymbol{n}}_k^{(i)}=g_k\left(\bar{\boldsymbol{l}}_i\right)$ for $k\in\{1,\dots,N_{\mathrm{R}}\}$ and $i\in\{1,\dots,N_{\mathrm{P}}\}$. The aim is to determine the optimal focus locations $\bar{\boldsymbol{l}}_1,\dots,\bar{\boldsymbol{l}}_{N_{\mathrm{P}}}$ to minimize the CRLB; that is,

$$\underset{\left\{\bar{\boldsymbol{l}}_i\right\}_{i=1}^{N_{\mathrm{P}}}}{\text{minimize}}\ \mathrm{trace}\{\mathbf{I}(\boldsymbol{x})^{-1}\} \tag{14}$$
$$\text{subject to}\ \tilde{\boldsymbol{n}}_k^{(i)}=g_k\left(\bar{\boldsymbol{l}}_i\right),\ k\in\{1,\dots,N_{\mathrm{R}}\},\ i\in\{1,\dots,N_{\mathrm{P}}\}$$

Since $\tilde{\boldsymbol{n}}_k^{(i)}$'s are replaced by $g_k\left(\bar{\boldsymbol{l}}_i\right)$ during the evaluations of the FIM, $\mathbf{I}(\boldsymbol{x})$ (see (7)–(12)), the CRLB is minimized over $3N_{\mathrm{P}}$ variables in this case, which is significantly simpler than the problem in (13) for practical IRS sizes. The problem in (14) can be solved via a global optimization tool such as particle swarm optimization (PSO) [40]. The IRS profiles obtained from the solution of (14) are called **focused IRS profiles** in the remainder of the manuscript.

In order to evaluate the performance of the proposed IRS profile selection strategy specified by (14) (i.e., focused IRS profiles), we can also introduce random and aligned IRS profiles as defined below:

Random IRS Profiles: For the random IRS profiles, we first set the limits for the azimuth and elevation angles of the IRS elements, i.e., mirrors, which are commonly mounted on a wall. These limits are chosen to ensure that the mirrors can be rotated robustly, precisely, and can accommodate the necessary mechanical systems for the selected angles. Let $(\zeta_{\min},\zeta_{\max})$ and $(\gamma_{\min},\gamma_{\max})$ denote the upper and lower limits for the azimuth and elevation angles, respectively. Then, the azimuth angles $\tilde{\zeta}_{i,k}$ and the elevation angles $\tilde{\gamma}_{i,k}$ for IRS element k and each IRS profile i are selected from independent uniform random variables as

[2] Pointing the LED towards the IRS may also prevent reflections from the other objects in the environment to reach the VLC receiver with significant power levels.

$\tilde{\zeta}_{i,k} \sim \mathcal{U}[\zeta_{\min}, \zeta_{\max}]$ and $\tilde{\gamma}_{i,k} \sim \mathcal{U}[\gamma_{\min}, \gamma_{\max}]$, respectively. Accordingly, the orientation vector of each IRS element in the random IRS profile can be defined as

$$\tilde{\boldsymbol{n}}_k^{(i)} = \begin{bmatrix} \cos\tilde{\gamma}_{i,k}\cos\tilde{\zeta}_{i,k} & -\sin\tilde{\zeta}_{i,k}\cos\tilde{\gamma}_{i,k} & \sin\tilde{\gamma}_{i,k} \\ \sin\tilde{\zeta}_{i,k} & \cos\tilde{\zeta}_{i,k} & 0 \\ -\sin\tilde{\gamma}_{i,k}\cos\tilde{\zeta}_{i,k} & \sin\tilde{\gamma}_{i,k}\sin\tilde{\zeta}_{i,k} & \cos\tilde{\gamma}_{i,k} \end{bmatrix} \mathbf{n}_0 \tag{15}$$

for $i \in \{1, \ldots, N_{\mathrm{P}}\}$ and $k \in \{1, \ldots, N_{\mathrm{R}}\}$, where $\mathbf{n}_0$ represents the orientation vector, which is perpendicular to the surface of the wall on which the IRS elements are mounted.

Aligned (Coordinated) IRS Profiles: The IRS elements can also have an aligned profile (also called coordinated in [41]). This IRS profile consists of IRS elements, the orientation vectors of which are the same as each other for all the IRS elements. The azimuth and elevation angles of the IRS elements (mirrors) are determined by the number of different IRS profiles that will be used for the position estimation process. The angles change linearly between different orientation profiles. For each orientation profile i, the azimuth and elevation angles for the IRS elements can be named as $\zeta^{(i)}$ and $\gamma^{(i)}$, respectively. Assuming that $\sqrt{N_{\mathrm{P}}}$ is an integer, these profiles can be formulated as follows for N_{P} different orientations:

$$\zeta^{(k)} = \zeta_{\min} + (k-1)\frac{\zeta_{\max} - \zeta_{\min}}{\sqrt{N_{\mathrm{P}}} - 1}, \ k \in \{1, \ldots, \sqrt{N_{\mathrm{P}}}\} \tag{16}$$

$$\gamma^{(j)} = \gamma_{\min} + (j-1)\frac{\gamma_{\max} - \gamma_{\min}}{\sqrt{N_{\mathrm{P}}} - 1}, \ j \in \{1, \ldots, \sqrt{N_{\mathrm{P}}}\} \tag{17}$$

$$\tilde{\boldsymbol{n}}_k^{(i)} = \begin{bmatrix} \cos\gamma^{(j)}\cos\zeta^{(k)} & -\sin\zeta^{(k)}\cos\gamma^{(j)} & \sin\gamma^{(j)} \\ \sin\zeta^{(k)} & \cos\zeta^{(k)} & 0 \\ -\sin\gamma^{(j)}\cos\zeta^{(k)} & \sin\gamma^{(j)}\sin\zeta^{(k)} & \cos\gamma^{(j)} \end{bmatrix} \mathbf{n}_0 \tag{18}$$

where $i = (j-1)\sqrt{N_{\mathrm{P}}} + k$, $k, j \in \{1, \ldots, \sqrt{N_{\mathrm{P}}}\}$, and $\mathbf{n}_0$ represents the orientation vector, which is perpendicular to the surface of the wall on which the IRS elements are mounted.[3]

Remark 3: In visible light systems, IRSs are commonly implemented in forms of intelligent mirror arrays or intelligent metasurface reflectors [42]. Although we consider a system model with an intelligent mirror array in this study, the results would also hold for intelligent metasurface reflectors when they are used to control directions of reflected signals (i.e., to perform anomalous reflection) [42]. □

For all three profile types considered in our manuscript, an equal component of the computational complexity comes from the computation required for the ML estimator in (6). In the formulation of the ML estimator, the surface integral originally required for evaluating the function $dH_{i,k}^{\mathrm{ref}}(\boldsymbol{x}, \tilde{\boldsymbol{n}}_k^{(i)})$ can be obtained by scaling with the constant area of the mirror under the assumption that the size of the mirror is relatively small with respect to the distance of the LED transmitter from the IRS. The computational complexity of this ML estimator is primarily determined by the double summation over N_{P}, the number of received signal power measurements, and N_{R}, the number of reflectors or reference points considered (please see (6)). For a given position $\boldsymbol{x}$, the complexity of evaluating the summation is $O(N_{\mathrm{P}} \times N_{\mathrm{R}})$. If the ML estimator is solved using an iterative optimization method, the overall computational complexity becomes $O(T_{\mathrm{ML}} \times N_{\mathrm{P}} \times N_{\mathrm{R}})$, where T_{ML} is the number of iterations required for convergence.

Additionally, for the focused profile, the algorithm requires the receiver to solve the problem of minimizing the CRLB expression over a $3 \times N_{\mathrm{P}}$ dimensional space as in (14). This involves finding the optimal set of focus points $\{\bar{\boldsymbol{l}}_i\}_{i=1,\ldots,N_{\mathrm{P}}}$ that minimize the trace of the inverse of the FIM $\mathbf{I}(\boldsymbol{x})$. The FIM itself is dependent on the partial derivatives of the received signal power with respect to the position $\boldsymbol{x}$, which are provided in (10)–(12), and its calculation has a complexity order of $O(N_{\mathrm{P}} \times N_{\mathrm{R}})$, as can be noted from (7)–(9). Hence, the complexity of solving (14) can be stated as $O(T_{\mathrm{foc}} \times N_{\mathrm{P}} \times N_{\mathrm{R}})$, where T_{foc} is the number of evaluations of the objective function in (14). (For example, if PSO is used with a swarm size of 50 and a maximum number of iterations of 500, then $T_{\mathrm{foc}} = 25000$ (cf. Section 5).) Overall, considering the calculation of the ML estimator and the optimization for the focused IRS profile, the total complexity order can be specified as $O((T_{\mathrm{ML}} + T_{\mathrm{foc}}) \times N_{\mathrm{P}} \times N_{\mathrm{R}})$, which highlights the added computational burden of solving the CRLB minimization before applying the ML estimation. Since the optimization problem for focused IRS profiles in (14) is solved over an $3N_{\mathrm{P}}$ dimensional space, it usually requires significantly more evaluations than that in the solution of the ML estimator in (6), which requires optimization over a three-dimensional space; i.e., $T_{\mathrm{foc}} \gg T_{\mathrm{ML}}$. Since the random and aligned IRS profiles do not require solving optimization problems, their complexity just comes from the ML estimator, i.e., $O(T_{\mathrm{ML}} \times N_{\mathrm{P}} \times N_{\mathrm{R}})$.[4]

4. Extensions

4.1. IRS profile selection without knowing position of VLC receiver

It is noted that setting the IRS profiles based on the proposed approach in (14) requires the knowledge of the position of the VLC receiver, which is not available in practice. In a tracking scenario, the position estimate in the previous time step can be used to select the IRS profiles via the proposed approach. If the position estimation is to be performed for the first time, aligned IRS profiles can be selected first, and an initial position estimation can be performed accordingly. Then, by considering the initial position estimate as the position of the VLC receiver, the optimization problem in (14) is solved to determine the new IRS profiles and the position estimation is performed again. This procedure can be repeated a number of times to improve the localization accuracy, depending on the availability of resources and the mobility of the VLC receiver.

Alternatively, IRS profiles can be selected for generic positions of the VLC receiver instead of its specific position at a given time. Assume that there exist prior information about the position of the VLC receiver such that $\Pr(\boldsymbol{x} = \boldsymbol{x}_j) = \pi_j$ for $j = 1, \ldots, N_{\mathrm{L}}$ with $\pi_j \in [0,1]$ and $\sum_{j=1}^{N_{\mathrm{L}}} \pi_j = 1$. That is, the VLC receiver can be at position $\boldsymbol{x}_j$ with probability π_j. In that case, the optimal focus locations can be chosen according to the average CRLB, which leads to the following problem (cf. (14)):

$$\underset{\{\bar{\boldsymbol{l}}_i\}_{i=1}^{N_{\mathrm{P}}}}{\text{minimize}} \ \sum_{j=1}^{N_{\mathrm{L}}} \pi_j \operatorname{trace}\{\mathbf{I}(\boldsymbol{x}_j)^{-1}\} \tag{19}$$
$$\text{subject to } \tilde{\boldsymbol{n}}_k^{(i)} = g_k(\bar{\boldsymbol{l}}_i),\ k \in \{1, \ldots, N_{\mathrm{R}}\},\ i \in \{1, \ldots, N_{\mathrm{P}}\}$$

where $g_k(\cdot)$'s denote the known mappings between the focus locations and the orientation vectors of the IRS elements [33, Sec. III]. The advantage of this approach is that the IRS profiles do not need to be updated for different positions of the VLC receiver, and the same design is used for a given environment. However, the resulting positioning accuracy can be inferior to the approach proposed in Section 3 (and that stated in the previous paragraph) for a given position of the VLC receiver.

4.2. Position estimation with a single LED when IRS is at the transmitter

In this study, the IRS is assumed to be between the transmitter and the receiver. However, it is also possible to employ an IRS at the trans-

[3] If $\sqrt{N_{\mathrm{P}}}$ is not an integer, then different numbers of angles can be chosen for azimuth and elevation angles.

[4] Although the approach in [33] is for the scenario with multiple LEDs, we can present its computational complexity for comparison purposes as follows: The complexity order of the ML estimator in [33] is proportional to the number of LEDs and the total number of IRS elements in the IRSs. To improve the accuracy, the IRS elements were directed towards the VLC receiver in [33] with a low complexity approach. In our manuscript, the aligned and random profiles also have low (negligible) complexity whereas the focused IRS profile has a higher complexity, as specified above.

mitter, which can be used to perform beam-steering towards specific directions [42]. In that case, a similar problem can be formulated to perform VLP with a single LED transmitter equipped with an IRS and a VLC receiver with a single photo-diode. In that scenario, we can effectively consider that the orientation vector of the LED can be adjusted. Suppose we set the orientation vector of the LED transmitter to N_{P} different values during the localization process, which are denoted by $\boldsymbol{n}^{(1)},\dots,\boldsymbol{n}^{(N_{\mathrm{P}})}$. Then, the VLC receiver can estimate its position based on the signals coming from the LED transmitter when the LED transmitter sets its orientation vector to these N_{P} predefined values. In this case, the received power for the ith orientation of the LED transmitter can be expressed as

$$P_{\mathrm{RX},i} = P_{\mathrm{TX}} H_i^{\mathrm{LOS}}(\boldsymbol{x}) + \eta_i \tag{20}$$

for $i = 1,\dots,N_{\mathrm{P}}$, where P_{TX} and η_i are as defined for (1), and $H_i^{\mathrm{LOS}}(\boldsymbol{x})$ is given by (cf. (2))

$$H_i^{\mathrm{LOS}}(\boldsymbol{x}) = \frac{(m+1)A\left((\boldsymbol{x}-\boldsymbol{l})^T\boldsymbol{n}^{(i)}\right)^m(\boldsymbol{l}-\boldsymbol{x})^T\bar{\boldsymbol{n}}}{2\pi\|\boldsymbol{x}-\boldsymbol{l}\|^{m+3}} \tag{21}$$

where $\boldsymbol{n}^{(i)}$ denotes the ith orientation vector for the LED transmitter. For the received powers in (20), the ML estimator can be derived as (cf. (6))

$$\hat{\boldsymbol{x}}_{\mathrm{ML}} = \arg\min_{\boldsymbol{x}} \sum_{i=1}^{N_{\mathrm{P}}} \frac{1}{\sigma_i^2}\left(P_{\mathrm{RX},i} - P_{\mathrm{TX}} H_i^{\mathrm{LOS}}(\boldsymbol{x})\right)^2 \tag{22}$$

and the FIM can be expressed as in (7) by updating $\frac{\partial h_i(\boldsymbol{x})}{\partial x_\ell}$ as (cf. (9))

$$\frac{\partial h_i(\boldsymbol{x})}{\partial x_\ell} = \frac{\partial H_i^{\mathrm{LOS}}(\boldsymbol{x})}{\partial x_\ell} \tag{23}$$

which can be calculated similarly to (10) by replacing $\boldsymbol{n}$'s with $\boldsymbol{n}^{(i)}$'s in that expression. Based on the CRLB expression that can be obtained from (7) and (23), the problem of determining optimal orientation vectors can be stated as follows:

$$\begin{aligned}&\underset{\boldsymbol{n}^{(1)},\dots,\boldsymbol{n}^{(N_{\mathrm{P}})}}{\text{minimize}}\ \operatorname{trace}\{\mathbf{I}(\boldsymbol{x})^{-1}\}\\ &\text{subject to } \|\boldsymbol{n}^{(i)}\| = 1,\ i \in \{1,\dots,N_{\mathrm{P}}\}\end{aligned} \tag{24}$$

This problem requires optimization over a $2N_{\mathrm{P}}$-dimensional space (by incorporating the constraints) and can be solved via global optimization tools such as PSO.

5. Simulation results

In this section, simulations are conducted to evaluate the performance of the proposed positioning approach for VLP in the presence of an IRS. A room with dimensions of $4\times4\times3$ meters (width, depth, and height, respectively) is considered as the simulation environment [33]. A single LED transmitter is positioned at the center of the room's ceiling, located at coordinates $\boldsymbol{l} = [0,0,3]^T$ meters. The LED is directed towards the center of the IRS (i.e., intelligent mirror array), characterized by the orientation vector $\boldsymbol{n} = [0,0.8,-0.6]^T$. The transmit power P_{TX} of the LED is set to 5 W and the Lambertian order is set as $m = 20$. The orientation vector of the VLC receiver is given by $\bar{\boldsymbol{n}} = [0,0,1]^T$, which is perpendicular to the room floor and faces upwards. The noise variances, σ_i^2, are assumed to be the same across different measurements obtained for various IRS profiles; that is, $\sigma_i^2 = \sigma^2$ for all $i \in \{1,\dots,N_{\mathrm{P}}\}$.

A three-dimensional depiction of the indoor simulation setup is presented in Fig. 2. The IRS is placed on one of the walls and arranged in a square grid format with dimensions $\sqrt{N_{\mathrm{R}}}\times\sqrt{N_{\mathrm{R}}}$, indicating the number of elements in rows and columns, respectively. Specifically, the number of IRS elements N_{R} is set to 441, each with 21 controllable mirrors in both columns and rows. The dimensions of the individual IRS elements (mirrors) within the IRS are set to a width w_k of 4 cm and a length l_k of 2 cm, resulting in a uniform surface area of $S_k = 8\,\mathrm{cm}^2$ for each IRS element. The horizontal distance h_d between the IRS elements and the vertical distance v_d are set to 2 cm and 1 cm, respectively, to prevent inter-element blockage. The spatial arrangement of the mirrors within the IRS is depicted in Fig. 3.

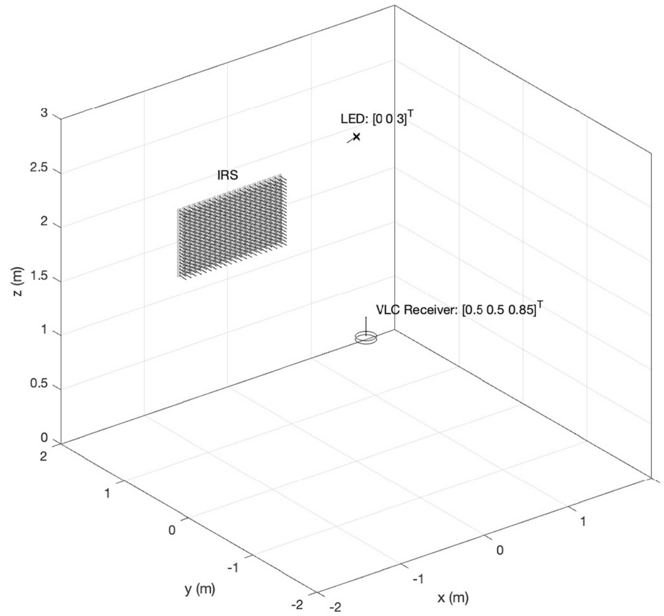

Fig. 2. The three-dimensional setup of the room used in the simulations. Gray rectangles on the wall represent the IRS elements (mirrors), with small black arrows indicating the orientation vectors of each IRS element. Additionally, the VLC receiver and the LED transmitter are shown, along with their respective orientation vectors.

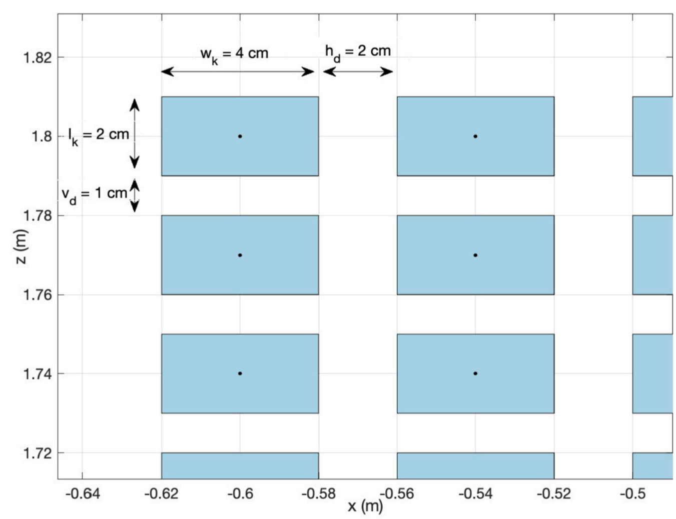

Fig. 3. A detailed view of the configuration of the IRS elements on the wall at $y = 2$ meters.

The reflectance coefficient of all the IRS elements is uniformly set to $\rho_k = 0.95$ (see (3)). Additionally, there are several parameters associated with the mirror elements of the IRS that influence the positioning accuracy. The fraction of the diffuse component (r_k) determines the ratio of diffuse reflections' power to the total reflected power, with values in the range of $[0,1]$ (see (3)). For the simulations, r_k is set to 0.5, implying an equal distribution between specular and diffuse reflections. Another significant parameter, the directivity of reflection (μ_k), is determined by the surface properties of the reflectors and affects the amount of reflected power (see (3)). We set μ_k to 5 for all k during the simulations.

Simulations are conducted utilizing the three IRS profile selection strategies delineated in Section 3. A consistent random seed of 42 is employed in MATLAB for the random IRS profiles, considering $N_\mathrm{P} = 9, 16, 25$ for the number of profiles.[5] The boundary angles of the uniform distribution, described in Section 3 as $\zeta_{\min}, \gamma_{\min}, \zeta_{\max}, \gamma_{\max}$, are specified by $-30°, -40°, 30°, 20°$, respectively, which are employed for generating the random and aligned IRS profiles. The selected angles are chosen to prevent signal transmission to unintended locations in both random and aligned IRS profile scenarios. This approach focuses on concentrating power within the potential search grid inside the room, thereby preserving the integrity of the information.

For deriving the focused IRS profiles, the problem in (14) is solved via the PSO algorithm, which is configured with a swarm size of 50 and a maximum number of iterations being 500. For a given value of N_P, each particle becomes a vector with a size of $3N_\mathrm{P}$ in the PSO algorithm, yielding the focusing locations at the end of optimization. The performance evaluation for employing different IRS profile selection strategies is conducted by considering various numbers of power measurements (i.e., IRS profiles), namely, $N_\mathrm{P} \in \{9, 16, 25\}$ in three sets of simulations.

For comparison of different IRS selection strategies, we both evaluate the performance of the ML estimator and the CRLB. The root mean-squared error (RMSE) of the ML estimator is calculated for different noise variances by performing 500 estimations for the position of the VLC receiver, which is located at $\mathbf{x} = [0.5, 0.5, 0.85]^T$ m. We first consider $N_\mathrm{P} = 9$ IRS profiles (i.e., measurements) and present the results in Fig. 4, which illustrates the RMSEs of the ML estimators and the CRLBs for the three IRS profile selection strategies with respect to $10\log_{10}(1/\sigma^2)$. Compared to the aligned and random IRS profiles, it can be seen that the focused IRS profiles, which are constructed by optimizing the focus locations, yield significantly lower RMSEs and CRLBs when the noise level is sufficiently low (equivalently, when the SNR is sufficiently high). It is also noted that the random IRS profiles lead to inferior performance and do not facilitate accurate localization for practical noise levels.[6] We repeat the same experiment also for $N_\mathrm{P} = 16$ and $N_\mathrm{P} = 25$, and present the results in Figs. 5 and 6, respectively. Again, the same behavior is observed and the focused IRS profiles achieve the highest accuracy. Also, as expected, the RMSE values decrease as N_P increases.

In order to investigate the reasons behind the favorable performance of the focused IRS profiles, we also illustrate the optimal focus locations yielded by the PSO algorithm as the solution of (14). In Figs. 7, 8, and 9, the focus locations for the focused IRS profiles are marked with the $\times$ signs for $N_\mathrm{P} = 9$, $N_\mathrm{P} = 16$, and $N_\mathrm{P} = 25$, respectively. It should be emphasized that since the noise variance σ^2 is just a scaling factor in the CRLB expression, the same focus locations are obtained via (14) for all values of σ^2. The investigation of Figs. 7–9 reveals that the focus locations tend to be clustered at several points inside the room adjacent to the walls. The locations of the centers of these clusters are also similar to each other for different values of N_P. This behavior of the optimal focus locations can be associated with spreading the focus centers of the clusters to some distant locations to improve the localization accuracy.

The effects of the physical parameters of the LED, photo-detector, and IRS elements should be discussed for further analysis of the results. The area of the photo-detector, A, and the area of the mirror elements are constant multipliers that scale the level of received signal power. Similar to the area parameters, the reflection coefficient ρ_k is a physical parameter of the mirror that can be considered a constant multiplier. These physical variables contribute to the total received power similarly as scale factors. Increasing these variables improves (reduces) the CRLB, as this leads to higher signal-to-noise ratios.

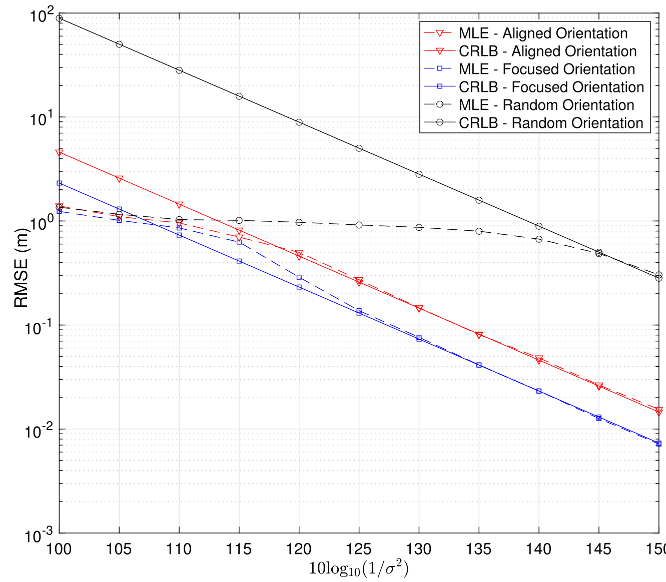

Fig. 4. RMSE and CRLB versus $10\log_{10}(1/\sigma^2)$ for random, aligned, and focused IRS profiles for $N_\mathrm{P} = 9$.

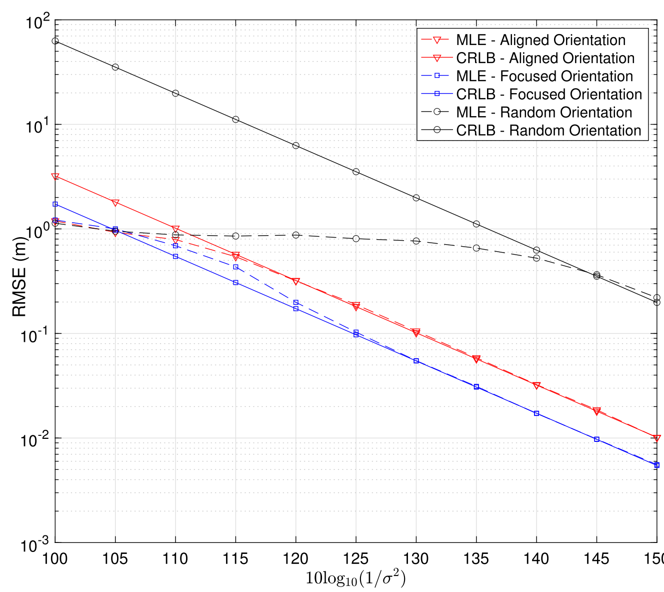

Fig. 5. RMSE and CRLB versus $10\log_{10}(1/\sigma^2)$ for random, aligned, and focused IRS profiles for $N_\mathrm{P} = 16$.

There are also three variables that depend on the spatial characteristics of the VLP setting. The Lambertian order m of the LED transmitter determines the directivity of the light rays emitted, which in turn affects the spatial concentration of the light power. We perform simulations using a similar setup with $N_\mathrm{P} = 9$ aligned IRS profiles, where $(r_k, \mu_k) = (0.5, 5)$, and obtain the RMSE and CRLB values for various values of m against the noise level. As shown in Fig. 10, the localization accuracy and the lower bound improve as the value of m increases. This can be explained by the fact that the majority of the location information is provided by the mirrors with glossy reflection. To avoid excessive scattering of the light, it must be kept more focused. Similar to the Lambertian order of the LED transmitter, the mirrors have the physical parameter μ_k, which is assumed to be identical for each element of the IRS. This parameter determines the directivity of the light reflected from the mirrors. Similar to m, increasing the parameter μ_k also improves localization performance. The parameter r_k is the portion of

[5] Changing the random seed does not affect the performance of the random IRS profile selection strategy significantly.

[6] The RMSEs of the ML estimators are lower than the CRLBs for high noise levels since during the calculation of the ML estimator in (6), the unknown position of the VLC receiver $\boldsymbol{x}$ is searched only over the possible locations in the room whereas no prior information about the position parameter is assumed in deriving the CRLB.

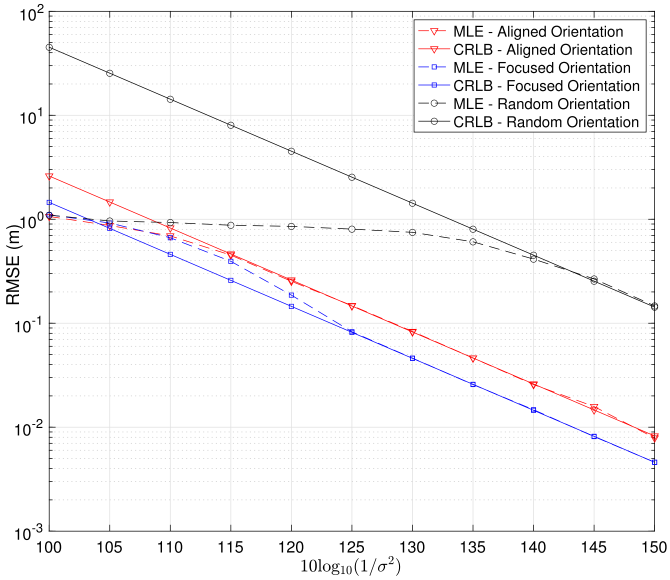

Fig. 6. RMSE and CRLB versus $10\log_{10}(1/\sigma^2)$ for random, aligned, and focused IRS profiles for $N_P = 25$.

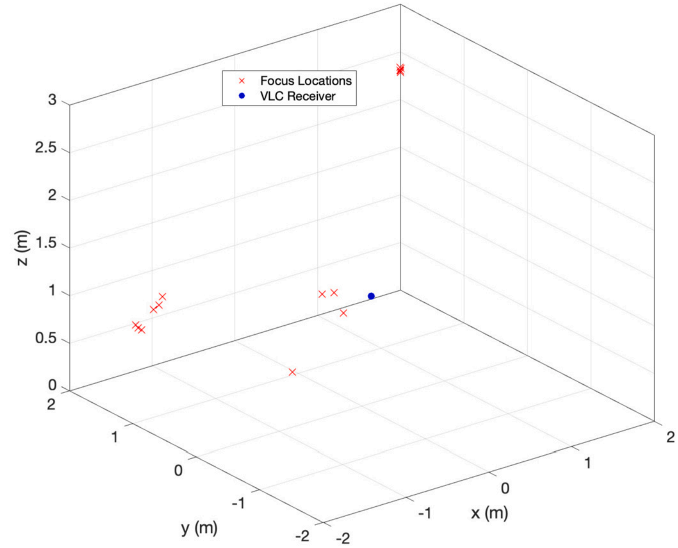

Fig. 8. Locations of the focus points (red) obtained from (14) for the focused IRS profiles strategy, where $N_P = 16$. The position of the VLC receiver (blue) is also illustrated while the LED and the IRS are not shown.

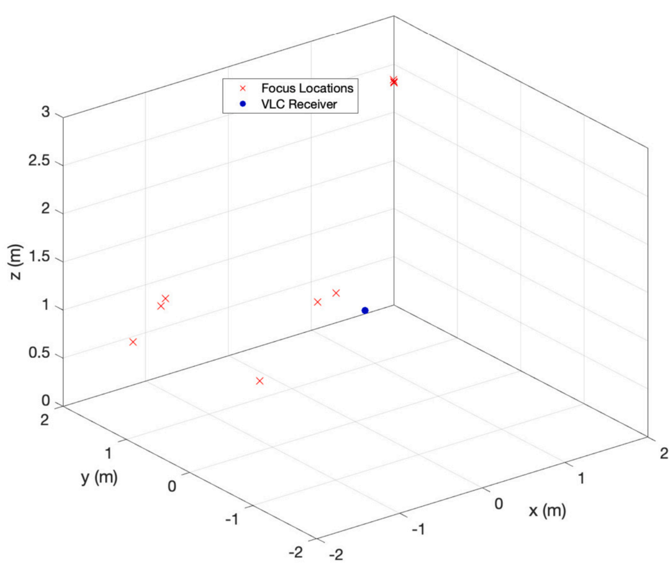

Fig. 7. Locations of the focus points (red) obtained from (14) for the focused IRS profiles strategy, where $N_P = 9$. The position of the VLC receiver (blue) is also illustrated while the LED and the IRS are not shown.

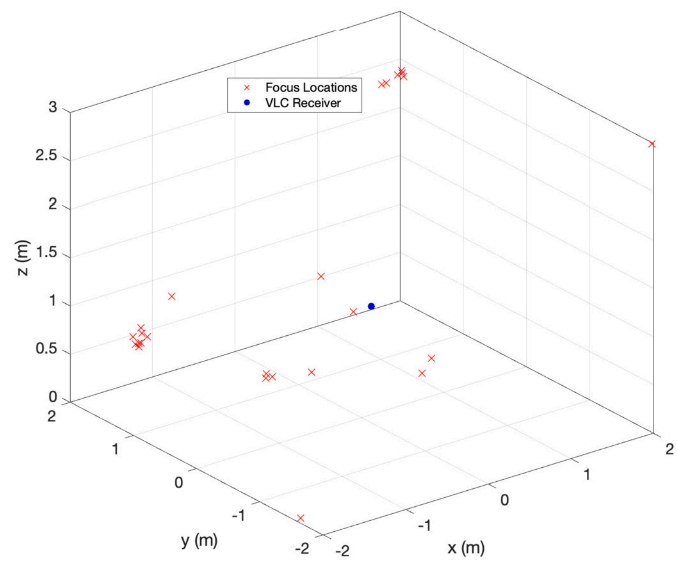

Fig. 9. Locations of the focus points (red) obtained from (14) for the focused IRS profiles strategy, where $N_P = 25$. The position of the VLC receiver (blue) is also illustrated while the LED and the IRS are not shown.

light that is reflected diffusively compared to the portion reflected specularly. As can be seen in Fig. 11, increasing μ_k or reducing r_k enhances the localization performance.

While increasing the physical parameters related to the directivity of the mirrors and the LED transmitter enhances localization performance, it is important to note that this improvement is only applicable when the receiver location is known. In practice, the position of the VLC receiver can be determined as described in Section 4.1 based on an initial localization of the VLC receiver, which benefits from less directive light. Therefore, choosing directivity parameters that are moderate, rather than extreme, may be more practical, as it balances the need for accurate localization with the initial requirements of the algorithm.

Another important physical parameter of the system is the size of the IRS elements (mirrors). In order to investigate the effects of this parameter, we perform simulations for the case of $N_P = 9$ with the aligned IRS profile. We vary both the vertical and horizontal distances between the mirrors, as well as their vertical and horizontal dimensions by taking the half and quarter of the original sizes illustrated in Fig. 3. The results are shown in Fig. 12, which shows that reducing the sizes of and the distances between the IRS elements negatively impacts the performance. This is because the size of each mirror element is related to several factors that influence the channel gain. Namely, increasing the area of the mirror array generally enhances the channel gain and the spatial coverage of the signals reflecting from the IRS.

6. Concluding remarks

We have proposed a VLP system consisting of a single LED transmitter, a VLC receiver with a single photo-diode, and an IRS. We have shown that by setting the orientation vectors of the IRS elements to a number of different values, called IRS profiles, and collecting power measurements for all profiles, position estimation can be performed. In addition, we have proposed a focusing approach for selecting IRS profiles in order to improve the localization accuracy. The proposed fo-

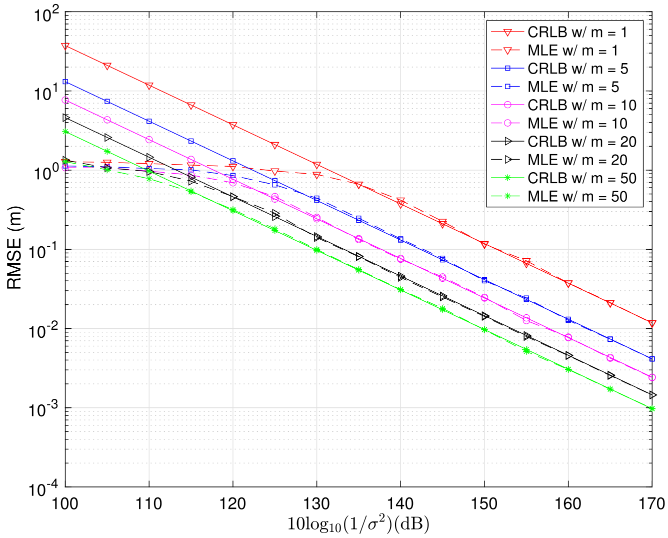

Fig. 10. RMSE and CRLB versus $10\log_{10}(1/\sigma^2)$ for the aligned profile with $N_P = 9$, $r_k = 0.5$, and $\mu_k = 5$, comparing different values of the Lambertian order (m).

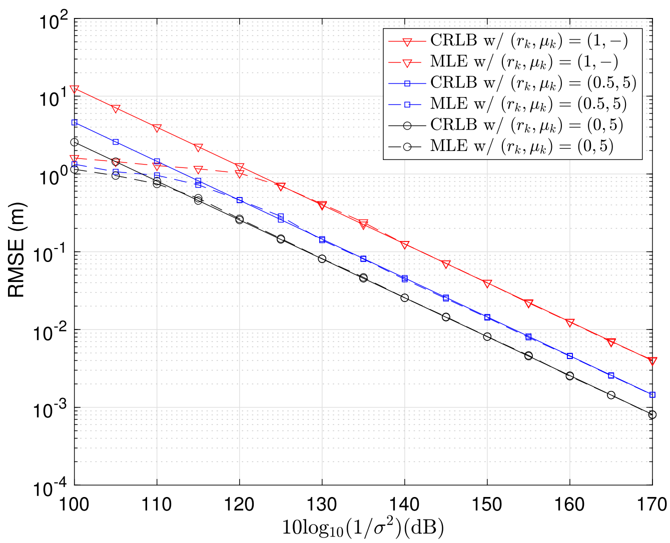

Fig. 11. RMSE and CRLB versus $10\log_{10}(1/\sigma^2)$ for the **aligned** profile with $N_P = 9$ and $m = 20$ comparing different values of (r_k, μ_k) pairs.

cused IRS profiles, which are obtained via CRLB minimization, have been shown to provide significant improvements in localization accuracy compared to the random and aligned IRS profiles. Furthermore, various discussions are provided for applying the proposed approach in practice, and extending the results to scenarios where the IRS is an integrated part of the transmitter.

CRediT authorship contribution statement

Efe Tarhan: Conceptualization, Methodology, Formal analysis, Software, Writing - Original Draft, Writing - Revised Draft. Furkan Kokdogan: Methodology, Formal analysis, Software, Review & Editing - Original Draft. Sinan Gezici: Conceptualization, Methodology, Writing - Original Draft, Writing - Revised Draft, Review & Editing, Revised Draft, Supervision.

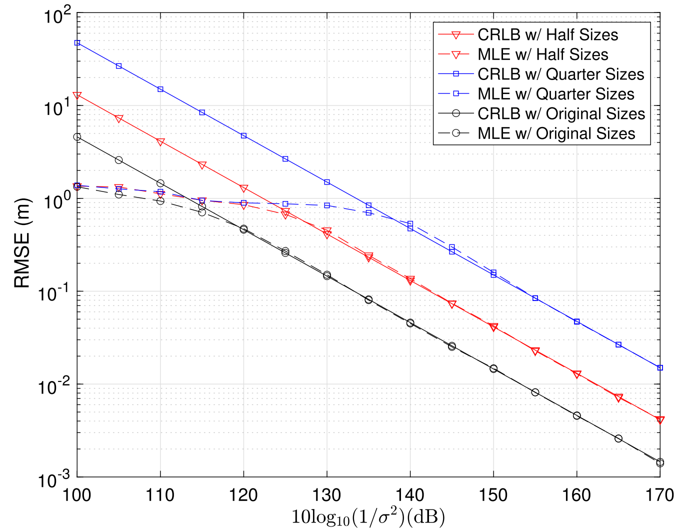

Fig. 12. Effects of changing the sizes of the IRS elements (mirrors).

Declaration of competing interest

The authors declare that they have no known competing financial interests or personal relationships that could have appeared to influence the work reported in this paper.

Data availability

No data was used for the research described in the article.

References

[1] C. Chen, W.-D. Zhong, D. Wu, On the coverage of multiple-input multiple-output visible light communications, J. Opt. Commun. Netw. 9 (9) (Sep. 2017) D31–D41.
[2] S. Shao, A. Khreishah, M. Ayyash, M.B. Rahaim, H. Elgala, V. Jungnickel, D. Schulz, T.D.C. Little, J. Hilt, R. Freund, Design and analysis of a visible-light-communication enhanced WiFi system, J. Opt. Commun. Netw. 7 (10) (Oct. 2015) 960–973.
[3] T. Komine, M. Nakagawa, Fundamental analysis for visible-light communication system using LED lights, IEEE Trans. Consum. Electron. 50 (1) (Feb. 2004) 100–107.
[4] A.T. Hussein, M.T. Alresheedi, J.M.H. Elmirghani, Fast and efficient adaptation techniques for visible light communication systems, J. Opt. Commun. Netw. 8 (6) (2016) 382–397.
[5] S. Rajagopal, R.D. Roberts, S.-K. Lim, IEEE 802.15.7 visible light communication: modulation schemes and dimming support, IEEE Commun. Mag. 50 (3) (2012) 72–82.
[6] J. Armstrong, Y. Sekercioglu, A. Neild, Visible light positioning: a roadmap for international standardization, IEEE Commun. Mag. 51 (12) (Dec. 2013) 68–73.
[7] Y. Hou, S. Xiao, H. Zheng, W. Hu, Multiple access scheme based on block encoding time division multiplexing in an indoor positioning system using visible light, J. Opt. Commun. Netw. 7 (5) (2015) 489–495.
[8] M. Yoshino, S. Haruyama, M. Nakagawa, High-accuracy positioning system using visible LED lights and image sensor, in: 2008 IEEE Radio and Wireless Symposium, 2008, pp. 439–442.
[9] I. Iddrisu, S. Gezici, Visible light positioning under luminous flux degradation of LEDs, arXiv:2312.07742, 2023.
[10] D. Karunatilaka, F. Zafar, V. Kalavally, R. Parthiban, LED based indoor visible light communications: state of the art, IEEE Commun. Surv. Tutor. 17 (3) (2015) 1649–1678.
[11] J. Luo, L. Fan, H. Li, Indoor positioning systems based on visible light communication: state of the art, IEEE Commun. Surv. Tutor. 19 (4) (2017) 2871–2893.
[12] M.F. Keskin, A.D. Sezer, S. Gezici, Localization via visible light systems, Proc. IEEE 106 (6) (June 2018) 1063–1088.
[13] H. Steendam, T.Q. Wang, J. Armstrong, Theoretical lower bound for indoor visible light positioning using received signal strength measurements and an aperture-based receiver, J. Lightwave Technol. 35 (2) (Jan 2017) 309–319.
[14] Z. Wang, Z. Liang, R. Liu, X. Li, H. Li, Design and performance analysis for indoor visible light positioning with single-LED and single-tilted-rotatable-PD, IEEE Trans. Instrum. Meas. (2024).
[15] B. Zhou, A. Liu, V. Lau, On the fundamental performance limit of visible light-based positioning, in: 13th International Conference on Signal Processing and Communication Systems (ICSPCS), 2019, pp. 1–6.

[16] E. Basar, M. Di Renzo, J. De Rosny, M. Debbah, M.-S. Alouini, R. Zhang, Wireless communications through reconfigurable intelligent surfaces, IEEE Access 7 (2019) 753–116 773.
[17] Q. Wu, R. Zhang, Intelligent reflecting surface enhanced wireless network via joint active and passive beamforming, IEEE Trans. Wirel. Commun. 18 (11) (2019) 5394–5409.
[18] T. Ma, Y. Xiao, X. Lei, W. Xiong, M. Xiao, Distributed reconfigurable intelligent surfaces assisted indoor positioning, IEEE Trans. Wirel. Commun. 22 (1) (2023) 47–58.
[19] A.M. Abdelhady, A.K.S. Salem, O. Amin, B. Shihada, M.-S. Alouini, Visible light communications via intelligent reflecting surfaces: metasurfaces vs mirror arrays, IEEE Open J. Commun. Soc. 2 (2021) 1–20.
[20] H. Abumarshoud, B. Selim, M. Tatipamula, H. Haas, Intelligent reflecting surfaces for enhanced NOMA-based visible light communications, in: IEEE International Conference on Communications (ICC), 2022, pp. 571–576.
[21] S. Malik, P. Saxena, Y.H. Chung, Performance analysis of a UAV-based IRS-assisted hybrid RF/FSO link with pointing and phase shift errors, J. Opt. Commun. Netw. 14 (4) (2022) 303–315.
[22] Q. Zhang, F. Yang, Z. Liu, S. Sun, H. Zhang, J. Song, Hardware implementation of a mirror array-based optical intelligent reflecting surface for VLC: prototype and experimental results, Opt. Express 32 (11) (May 2024) 252–19 264.
[23] A. Nasri, A.H.A. Bafghi, M. Nasiri-Kenari, Wireless localization in the presence of intelligent reflecting surface, IEEE Wirel. Commun. Lett. 11 (7) (2022) 1315–1319.
[24] M. Ammous, S. Valaee, Cooperative positioning with the aid of reconfigurable intelligent surfaces and zero access points, in: 2022 IEEE 96th Vehicular Technology Conference (VTC2022-Fall), 2022, pp. 1–5.
[25] Y. Liu, E. Liu, R. Wang, Y. Geng, Reconfigurable intelligent surface aided wireless localization, in: IEEE International Conference on Communications (ICC), 2021, pp. 1–6.
[26] N. Afzali, M.J. Omidi, K. Navaie, N.S. Moayedian, Low complexity multi-user indoor localization using reconfigurable intelligent surface, in: 2022 30th International Conference on Electrical Engineering (ICEE), 2022, pp. 731–736.
[27] T. Zhou, K. Xu, Z. Shen, W. Xie, D. Zhang, J. Xu, Aoa-based positioning for aerial intelligent reflecting surface-aided wireless communications: an angle-domain approach, IEEE Wirel. Commun. Lett. 11 (4) (2022) 761–765.
[28] B. Chen, J. Jiang, W. Guan, S. Wen, J. Li, Y. Chen, Performance comparison and analysis on different optimization models for high-precision three-dimensional visible light positioning, Opt. Eng. 57 (1) (2018) 12.
[29] X. Meng, C. Jia, C. Cai, F. He, Q. Wang, Indoor high-precision 3D positioning system based on visible-light communication using improved whale optimization algorithm, Photonics 9 (2) (2022).
[30] R. Alghamdi, R. Alhadrami, D. Alhothali, H. Almorad, A. Faisal, S. Helal, R. Shalabi, R. Asfour, N. Hammad, A. Shams, N. Saeed, H. Dahrouj, T.Y. Al-Naffouri, M.-S. Alouini, Intelligent surfaces for 6G wireless networks: a survey of optimization and performance analysis techniques, IEEE Access 8 (2020) 795–202 818.
[31] Q. Wu, J. Zhang, J. Guo, Capacity maximization for reconfigurable intelligent surface-aided miso visible light communications, Photonics 9 (7) (2022).
[32] T. Yang, P. Wang, G. Li, H. Wang, S. Li, H. Shi, H. He, F. Shi, S. Chi, Average signal-to-noise ratio maximization for an intelligent reflecting surface and angle diversity receiver jointly assisted indoor visible light communication system, Appl. Opt. 61 (35) (Dec 2022) 390–10 399.
[33] F. Kokdogan, S. Gezici, Intelligent reflecting surfaces for visible light positioning based on received power measurements, IEEE Trans. Veh. Technol. (2024) 1–14.
[34] I. Iddrisu, S. Gezici, Visible light positioning with intelligent reflecting surfaces under mismatched orientations, arXiv:2407.10612, 2024.
[35] M.F. Keskin, A.D. Sezer, S. Gezici, Optimal and robust power allocation for visible light positioning systems under illumination constraints, IEEE Trans. Commun. 67 (1) (2019) 527–542.
[36] O. Gonzalez, S. Rodriguez, R. Perez-Jimenez, B. Mendoza, A. Ayala, Error analysis of the simulated impulse response on indoor wireless optical channels using a Monte Carlo-based ray-tracing algorithm, IEEE Trans. Commun. 53 (1) (2005) 124–130.
[37] E. Gonendik, S. Gezici, Fundamental limits on RSS based range estimation in visible light positioning systems, IEEE Commun. Lett. 19 (12) (2015) 2138–2141.
[38] J.M. Kahn, J.R. Barry, Wireless infrared communications, Proc. IEEE 85 (2) (Feb. 1997) 265–298.
[39] H.V. Poor, An Introduction to Signal Detection and Estimation, 2nd ed., Springer-Verlag, New York, 1994.
[40] M. Clerc, Particle Swarm Optimization, Wiley-ISTE, 2006.
[41] S. Aboagye, T.M.N. Ngatched, O.A. Dobre, A.R. Ndjiongue, Intelligent reflecting surface-aided indoor visible light communication systems, IEEE Commun. Lett. 25 (12) (2021) 3913–3917.
[42] S. Aboagye, A.R. Ndjiongue, T.M.N. Ngatched, O.A. Dobre, H.V. Poor, RIS-assisted visible light communication systems: a tutorial, IEEE Commun. Surv. Tutor. 25 (1) (2023) 251–288.

Efe Tarhan received the bachelor's degree in Electrical and Electronics Engineering from Bilkent University in Ankara, Türkiye, in 2024 and is currently pursuing a master's degree in Communication Systems at École Polytechnique Fédérale de Lausanne in Lausanne, Switzerland. His research interests include image processing, machine learning, and wireless communication systems.

Furkan Kokdogan received the B.S., M.S., and Ph.D. degrees from the Department of Electrical and Electronics Engineering, Bilkent University, Ankara, Türkey, in 2015, 2017, and 2023, respectively. He is currently with ASML Netherlands B.V., Veldhoven, where he has been an Embedded Logic and Firmware Designer since 2022. His research focuses on visible light positioning.

Sinan Gezici received the B.Sc. degree in electrical and electronics engineering from Bilkent University, Ankara, Türkey, in 2001, and the Ph.D. degree in electrical engineering from Princeton University, Princeton, NJ, USA, in 2006. From 2006 to 2007, he was with Mitsubishi Electric Research Laboratories, Cambridge, MA, USA. Since 2007, he has been with the Department of Electrical and Electronics Engineering, Bilkent University, where he is currently a Professor. His research interests include the areas of detection and estimation theory, wireless communications, and localization systems. Among his publications in these areas is the book Ultra-wideband Positioning Systems: Theoretical Limits, Ranging Algorithms, and Protocols (Cambridge University Press, 2008). Dr. Gezici has been an Associate Editor for IEEE Transactions on Vehicular Technology, IEEE Transactions on Communications, IEEE Wireless Communications Letters, and Journal of Communications and Networks.